Demonstration of AlGaN-on-AlN p-n Diodes with Dopant-free Distributed Polarization Doping

Takeru Kumabe, *Graduate Student Member, IEEE*, Akira Yoshikawa, Seiya Kawasaki, *Graduate Student Member, IEEE*, Maki Kushimoto, Yoshio Honda, Manabu Arai, *Member, IEEE*, Jun Suda, *Senior Member, IEEE*, and Hiroshi Amano

***Abstract*— Nearly ideal vertical $Al_xGa_{1-x}N$ ($0.7 \leq x < 1.0$) p-n diodes are fabricated on an AlN substrate. Distributed polarization doping (DPD) was employed for both p-type and n-type layers of the p-n junction, instead of conventional impurity doping, to overcome the major bottleneck of AlN-based material: the control of conductivity. Capacitance–voltage measurements revealed that the net charge concentration agreed well with the DPD charge concentration expected from the device layer structure. The fabricated devices exhibited a low turn-on voltage of 6.5 V, a low differential specific ON-resistance of 3 mΩ cm^2, electroluminescence (maximum at 5.1 eV), and an ideality factor of 2 for a wide range of temperatures (room temperature–573 K). Moreover, the breakdown electric field was 7.3 MV cm^{-1}, which was almost twice as high as the reported critical electric field of GaN at the same doping concentration. These results clearly demonstrate the usefulness of DPD in the fabrication of high-performance AlN-based power devices.**

***Index Terms*— Aluminium nitride (AlN), distributed polarization doping (DPD), vertical p-n diode.**

I. Introduction

AlN and high-Al-content AlGaN are in the spotlight as materials for next-generation high-power devices thanks to their large energy bandgap (up to 6 eV) and high critical electric field (expected to be as high as 15 MV cm^{-1}) [1], [2]. In recent years, high-quality AlN substrates with low threading dislocation densities ($< 10^4$ cm^{-2}) have become commercially available, attracting attention for their potential use in vertical power devices [3]–[6]. However, even with the utilization of these high-quality AlN substrates, AlN-based vertical devices with ideal electrical properties have yet to be realized [7]–[9]. A major technical challenge for these devices is achieving controlled conductivity across a broad range. Specifically, the large ionization energy of the Si donor (280 meV) and the Mg acceptor (630 meV) in AlN poses significant difficulties in obtaining conductive layers at room temperature (RT) [10]–[14].

Distributed polarization doping (DPD), initially proposed and demonstrated by Jena *et al.* in 2002, is in the spotlight as a unique doping technology for nitride semiconductors [15]. Relying on the polarization effect in nitride semiconductors, DPD induces mobile electrons and holes solely through the compositional grading of nitride semiconductor alloys, thereby eliminating the need for impurity doping. This approach presents a promising solution to the challenges of conductivity control in AlN-based materials. To date, we have extensively studied GaN-based vertical p-n diodes formed by dopant-free DPD and demonstrated excellent electrical properties such as ideal breakdown electric field, high hole mobility, as well as longer electron lifetime and larger diffusion coefficient than those of p-GaN:Mg [16]–[18]. Moreover, our group employed DPD for the p-type cladding layer of an AlN-based laser diode to increase its conductivity and transparency. As a result, we successfully demonstrated the fabrication of AlN-based laser diodes with the capability of RT continuous-wave lasing at UV-C wavelengths [19]. Although this achievement shows the great potential of DPD to overcome the challenges of AlN-based materials, such successes have not been realized in other AlN-based device applications. Furthermore, the absence of devices with desired electrical characteristics also limits our understanding of the properties of AlN-based materials.

From both application and fundamental research perspectives, p-n diodes (PNDs) are critical components in semiconductor technology. However, for AlGaN with an AlN mole fraction exceeding 30%, PNDs that exhibit ideal electrical characteristics have not yet been realized using conventional impurity doping technology [12], [20]–[24]. In this study, we demonstrated the fabrication of AlN-based near-ideal vertical p-n diodes utilizing dopant-free DPD for both p-type and n-type layers of the p-n junction. Specifically, capacitance–voltage (C–V) measurements revealed that the net charge concentration is almost equal to that expected from the measured compositional gradient. Forward-biased current density–voltage (J–V) characteristics showed an ideality factor of around 2.0 for a wide range of temperatures, suggesting recombination current as typical p-n diodes. For reverse-biased J–V characteristics, the estimated parallel-plane breakdown electric field is greater than 7 MV cm^{-1}, despite the absence of an edge termination structure.

Takeru Kumabe, Seiya Kawasaki, and Maki Kushimoto are with the Department of Electronics, Nagoya University, Nagoya 464-8603, Japan (e-mail: kumabe@nagoya-u.jp).

Akira Yoshikawa is with the Advanced Devices Technology Center, Asahi Kasei Corporation, Tokyo 100-0006, Japan. He is also with the Institute of Materials and Systems for Sustainability, Nagoya University, Nagoya 464-8601, Japan.

Yoshio Honda, Manabu Arai, Jun Suda, and Hiroshi Amano are with the Institute of Materials and Systems for Sustainability, Nagoya University, Nagoya 464-8601, Japan.

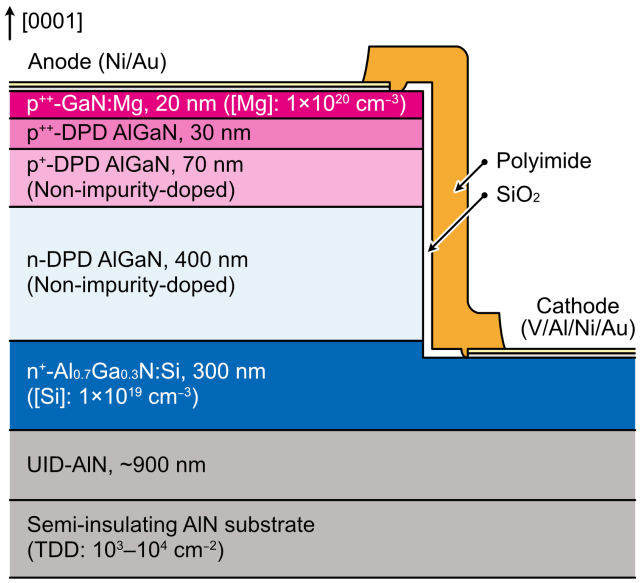

Fig. 1. Schematic cross-sectional view of a fabricated p^+-n diode. The AlN mole fraction (x) is linearly graded along the [0001] axis in the DPD layers.

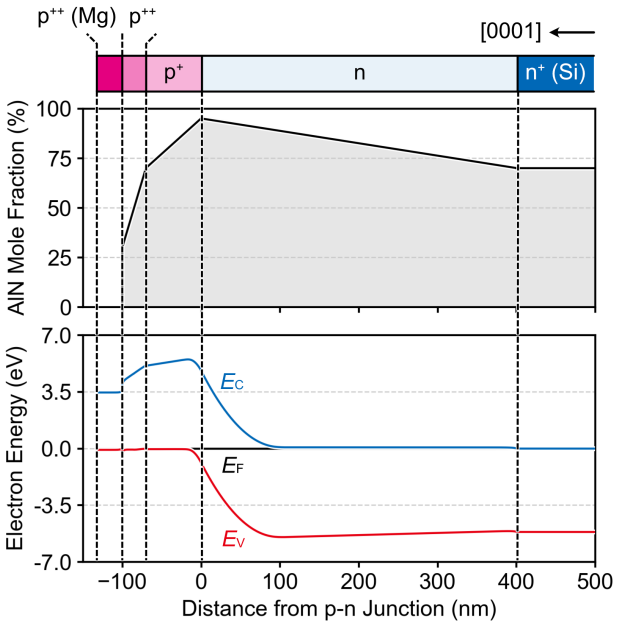

Fig. 2. AlN mole fraction distribution in the [0001] direction and energy-band diagram for the fabricated p^+-n diode structure. E_C, E_F, and E_V represent the conduction band minimum, the Fermi energy, and the valence band maximum, respectively.

II. Experiment

Fig. 1 illustrates the schematic cross-sectional view of a fabricated p^+-n diode. The AlN mole fraction (x) distribution in the [0001] direction and the corresponding energy-band diagram for this structure are also shown in Fig. 2. The device layer structure was grown by metal-organic vapor phase epitaxy (MOVPE) on a (0001)-plane semi-insulating AlN substrate. The AlN substrate was prepared by the physical vapor transport method, and its threading dislocation density (TDD) was on the order of 10^3–10^4 cm^{-2} [25]. The layers on the top of the substrate are unintentionally doped (UID)-AlN (900 nm), n^+-$Al_{0.7}Ga_{0.3}N$:Si ([Si]: 1×10^{19} cm^{-3}, 300 nm), n-DPD AlGaN (non-impurity doped, 400 nm), p^+-DPD AlGaN (non-impurity doped, 70 nm), p^{++}-DPD AlGaN (30 nm), and p^{++}-GaN:Mg ([Mg]: 1×10^{20} cm^{-3}, 20 nm). The x values in n-DPD AlGaN and p-DPD AlGaN were linearly graded from 70% to 95% along the [0001] direction, and the profile is asymmetrical to the junction plane to form the one-sided abrupt p^+-n junction structure. The expected average negative and positive DPD charge concentrations (N^-_{DPD} and N^+_{DPD}) for the p^+-DPD AlGaN and n-DPD AlGaN layers are 1.8×10^{18} cm^{-3} and 2.6×10^{17} cm^{-3}, respectively. The detailed method, including equations and material parameters, to calculate DPD charge concentrations is summarized in our previous report [16]. Furthermore, in p^{++}-DPD AlGaN, the x value was linearly graded from 70% to 30% along the [0001] direction, improving the p-type ohmic contact.

After the growth phase, diodes were fabricated through a series of processes. Initially, the p^{++}-GaN:Mg layer was activated (dehydrogenated) by annealing in an N_2 ambient at 973 K for 5 min. The vertical mesa structure was then defined by a combination of Cl_2-based inductively coupled plasma–reactive ion etching (ICP–RIE) and wet etching in a 25% solution of tetramethylammonium hydroxide (TMAH) at 353 K for 15 min [26]. The two-step ICP–RIE was used to minimize dry-etching-induced damage and improve the cathode ohmic contact citeKumabe2021. After protecting the device surface with a SiO_2 layer deposited by PECVD, a V/Al/Ni/Au stack was deposited and sintered at 1023 K for 2 min in an N_2 ambient to form the cathode ohmic electrode. Additionally, a Ni/Au stack was deposited and sintered at 789 K for 5 min in an O_2 ambient to serve as the anode ohmic electrode. The fabrication process was completed after depositing a Ti/Au stack on the electrode areas for probing and passivating the surface with polyimide.

X-ray diffraction reciprocal space mapping (XRD-RSM) measurement was conducted to examine the pseudomorphic growth and the minimum AlN mole fraction of the DPD layers. Secondary ion mass spectrometry (SIMS) measurement was also carried out to characterize the depth profiles of the AlN mole fraction and residual impurity concentrations around the p^+-n junction. Furthermore, *C–V* and *J–V* measurements were conducted to characterize the space charge profile and carrier transport properties of the fabricated diodes, respectively. The reverse current leakage mechanism was also investigated by photo emission microscopy and transmission electron microscopy (TEM) measurements.

III. Results and Discussion

A. Structural Properties

Fig. 3 shows the XRD-RSM of the $(\bar{1}\bar{1}24)$ plane for the prepared sample. Continuous AlGaN peaks, which are unique to compositionally graded AlGaN layers, could be observed in addition to the AlN peak. These AlGaN peaks aligned

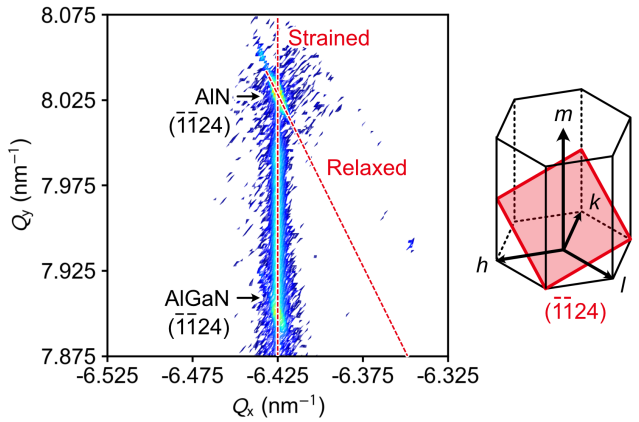

Fig. 3. XRD-RSM of the $(\bar{1}\bar{1}\mathbf{24})$ plane for the prepared sample. The inset shows the $(\bar{1}\bar{1}\mathbf{24})$ plane in wurtzite crystal. The peak under the "Relaxed" line originated from an AlN substrate, not a relaxed AlGaN layer.

precisely with the AlN peak in the in-plane (Q_x) direction, confirming that the DPD layers were pseudomorphically grown on the AlN substrate. The maximum and minimum values of x (x_{Max} and x_{Min}) were extracted as 95% and 70%, respectively, confirming that the layer structure depicted in Fig. 1 was grown as intended.

The depth profiles of Si, Mg, C, O, and Fe concentrations determined by SIMS are shown in Fig. 4(a). The detection limits were 2×10^{16} cm^{-3} for Si, 4×10^{15} cm^{-3} for Mg, 1×10^{16} cm^{-3} for C and O, as well as 5×10^{14} cm^{-3} for Fe. Since the growth conditions were carefully optimized to reduce residual impurities, their concentrations were below 5×10^{16} cm^{-3} in the n-DPD AlGaN layers, which were close to the detection limits. Fig. 4(b) shows the depth profile of the AlN mole fraction (x) determined by SIMS, which was corrected to analyze alloy composition quantitatively. x was linearly graded along the depth direction of the entire p-n junction. The expected N^{-}_{DPD} and N^{+}_{DPD} values calculated with respect to the gradient of x are plotted on the right axis [$N = q^{-1}dP(w)/dw$, where q is the elementary charge, P is the sum of spontaneous and piezoelectric polarizations, and w is the depth coordinate]. The average values of N^{-}_{DPD} and N^{+}_{DPD} were 1.8×10^{18} cm^{-3} and 2.6×10^{17} cm^{-3}, respectively. Note that the TEM analysis confirmed that the thicknesses of p^{+}-DPD AlGaN and n-DPD AlGaN layers determined by the SIMS measurement are accurate. This result indicates that the device layer structure has been successfully fabricated as designed.

B. Electrical Properties

Fig. 5 shows the $1/C^2$–V characteristics of the fabricated diode. The fabricated diode exhibited almost linear characteristics owing to the uniformly doped n-DPD AlGaN layer. The built-in potential (V_{bi}) extracted by linear extrapolation was 7.6 V, which was close to that expected in AlN-based p-n diodes (around 6 V) on the basis of the bandgap energy of Al(Ga)N. The net charge concentration (N) in the n-DPD AlGaN layer extracted from the C–V characteristics is also

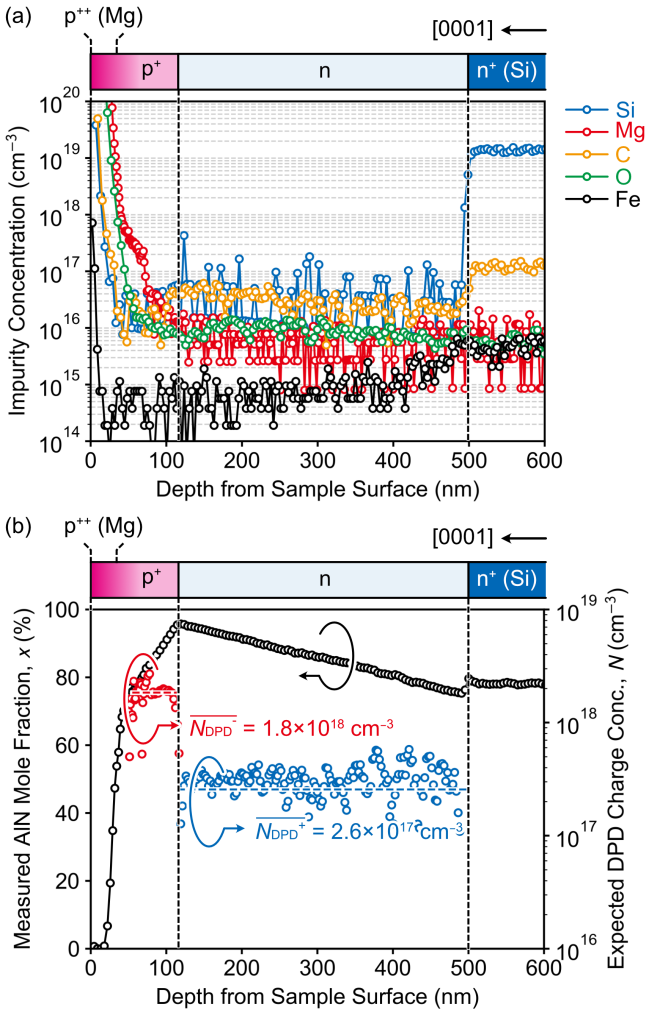

Fig. 4. (a) Depth profiles of Si, Mg, C, O, and Fe concentrations determined by SIMS. The detection limits were $\mathbf{2 \times 10^{16}}$ cm^{-3} for Si, $\mathbf{4 \times 10^{15}}$ cm^{-3} for Mg, $\mathbf{1 \times 10^{16}}$ cm^{-3} for C and O, as well as $\mathbf{5 \times 10^{14}}$ cm^{-3} for Fe. (b) Depth profile of x determined by SIMS (left) and expected DPD charge concentration (right).

shown in Fig. 6. The average value of N was 2.3×10^{17} cm^{-3}, which agrees well with the expected $N^{+}_{\mathrm{DPD}}N^{-}_{\mathrm{DPD}}/(N^{+}_{\mathrm{DPD}} + N^{-}_{\mathrm{DPD}})$ of 2.3×10^{17} cm^{-3} calculated considering the depth profile of x as shown in Fig. 4(b). Although voltage drop due to the high spreading resistance of the n^{+}-AlGaN:Si layer potentially led to the overestimation of V_{bi} and depletion width (w), the C–V measurement proved that the device has the designed structure (doping profile) from the viewpoint of electrical properties.

The forward-biased J–V characteristics of a fabricated diode measured at RT are shown in Fig. 7(a). The device exhibited a turn-on voltage (V_{th}) of 6.5 V and a minimum differential specific ON-resistance (r) of 3 mΩ cm^2, which are the smallest among the ever-reported AlN-based p-n diodes. Moreover, a comparison of 100 μm diameter and 200 μm diameter devices suggested the "actual" active region is restricted to the mesa periphery. Fig. 7(b) shows the photo emission microscopy image of a fabricated "typical" diode under forward-biased voltage (V_{F}) of 5.0 V [not the same diode as that shown

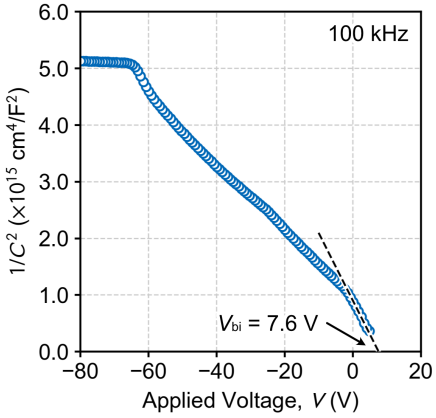

Fig. 5. $1/C^2$–V characteristics of the fabricated diode measured. AC frequency of this measurement was set to 100 kHz.

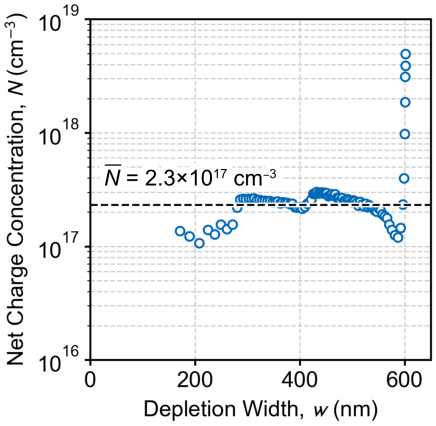

Fig. 6. Depth profile of net charge concentration (N) in the n-DPD AlGaN layer extracted from the C–V characteristics.

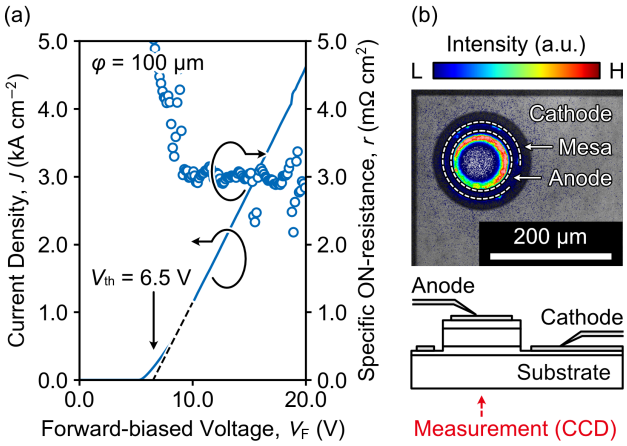

Fig. 7. (a) Forward-biased J–V characteristics of the fabricated diode at RT. Specific ON-resistance (r) is also plotted on the right axis. "ϕ" denotes device diameter. The variation in r value within this chip is approximately ±7%, as determined from testing a total of 12 devices (each with a diameter of 200 μm, not 100 μm). (b) Photo emission microscopy image of a fabricated "typical" diode under forward-biased voltage (V_F) of 5.0 V. The inset shows the measurement setup.

in Fig. 7(a)]. In this figure, areas with a relatively higher current density are presented in warm colors, whereas those with a lower current density are depicted in cool colors (or not painted). The actual active region is found to extend only about 20 μm inward from the anode electrode edge, suggesting that the spreading resistance in the n$^+$-$Al_{0.7}Ga_{0.3}N$:Si layer is the limiting factor for the ON-resistance. To quantitatively evaluate the limiting factor, specific contact resistances on the p^{++}-GaN:Mg and n$^+$-$Al_{0.7}Ga_{0.3}N$:Si layers, along with the sheet resistance of the n$^+$-$Al_{0.7}Ga_{0.3}N$:Si layer, were determined using circular transmission line model (TLM) test structures. The current–voltage (I–V) and resistance–gap distance (R_T–d) characteristics of fabricated circular TLM test structures are shown in Figs. 8(a) and 8(b). The I–V characteristics for both n-type and p-type contacts demonstrated nearly ohmic behavior, with total resistance showing a proportional relationship to the gap distance. The specific contact resistance (ρ_c) and sheet resistance (R_{sh}) were determined as 1.9×10^{-6} Ωcm^2 and 4.7×10^2 Ω/□ for n$^+$-$Al_{0.7}Ga_{0.3}N$:Si, as well as 4.5×10^{-4} Ω cm^2 and 1.3×10^5 Ω/□ for p^{++}-GaN:Mg, respectively. Moreover, the resistivity of n-DPD AlGaN and p-DPD AlGaN is estimated to be 0.23 and 0.34 Ωcm, based on the determined N^+_{DPD} and N^-_{DPD} values of 2.6×10^{17} and 1.8×10^{18} cm^{-3}, combined with assumed mobilities of $\mu_n = 100$ and $\mu_p = 10$ cm^{2}V^{-1}s^{-1}. Taking into account these values and the device geometry ($\phi = 100$ μm), the resistance contributions were calculated as 12 Ω for the p-type contact resistance (34% of the total), 3.1×10^{-2} Ω for the p-DPD AlGaN layer, 0.12 Ω for the n-DPD AlGaN layer, 22 Ω for the spreading resistance in the n$^+$-$Al_{0.7}Ga_{0.3}N$:Si layer (65% of the total), and 2.5×10^{-3} Ω for the n-type contact resistance, leading to a total resistance of 34 Ω. The total calculated resistance (34 Ω) aligns closely with the experimental ON-resistance of 38 Ω. As a result, the spreading resistance of the n$^+$-$Al_{0.7}Ga_{0.3}N$:Si layer, whose thickness is currently constrained by the critical thickness, is considered to be the primary limiting factor for the ON-resistance in the fabricated diodes.

Additionally, electroluminescence (EL) was observed under turn-on conditions. Fig. 9 shows EL spectra of the fabricated diode taken from the back side of the substrate. The EL emission increased with increasing current, suggesting that both electrons and holes contribute to the conduction as typical p-n junctions. Photons with energies higher than 5.13 eV are absorbed in the n$^+$-$Al_{0.7}Ga_{0.3}N$ layer, which has the smallest bandgap across the optical path.

Furthermore, the temperature-dependent J–V characteristics of the diodes were investigated in the temperature range of RT–573 K, as shown in Fig. 10. The forward J–V characteristics showed an exponential relationship, with the V_{th} tending to decrease with increasing temperature. In typical p-n junctions, the forward-biased carrier transport properties are described by the recombination-diffusion current model. The extent to which the experimental values fit this model is discussed using the ideality factor defined as

$$n = \frac{q}{k_B T}\left[\frac{d\ln(J)}{dV}\right]^{-1}, \quad 1 \le n \le 2. \tag{1}$$

Here, k_B is the Boltzmann constant, and T is temperature. The temperature-dependent n values are plotted in Fig. 11.

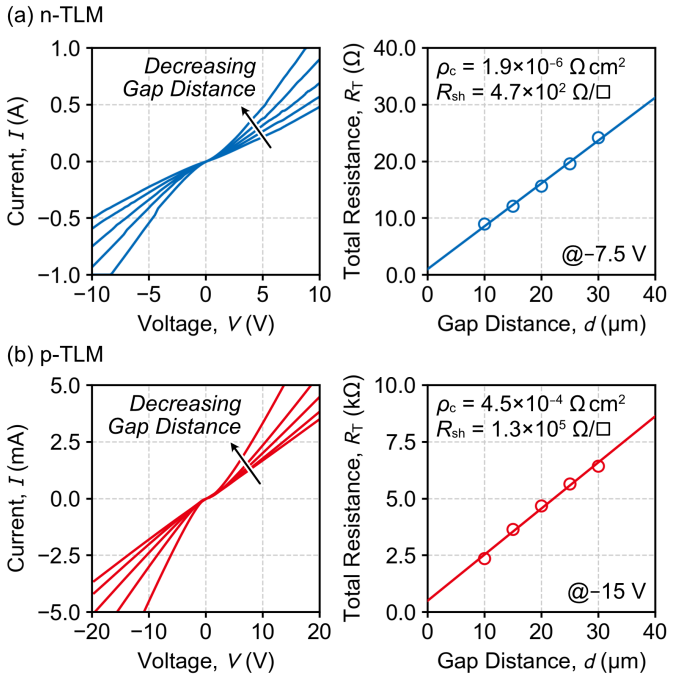

Fig. 8. Current–voltage (*I*–*V*) and total resistance–gap distance ($\boldsymbol{R_T}$–$\boldsymbol{d}$) characteristics of circular TLM test structures fabricated on (a) n-type and (b) p-type contact layers. $\boldsymbol{\rho_c}$ and $\boldsymbol{R_{sh}}$ indicate specific contact resistance and sheet resistance, respectively. The total resistance was extracted at a higher voltage, taking into account the measurement conditions of forward-biased *J*–*V* characteristics.

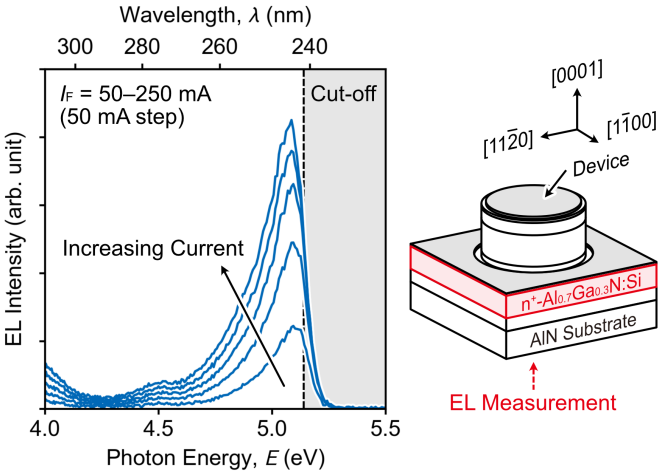

Fig. 9. EL spectra of the fabricated diode under various forward-bias conditions. The inset shows the bird's eye view illustration of the measurement. Photons with energies higher than 5.13 eV are absorbed in the n$^+$-$\mathbf{Al_{0.7}Ga_{0.3}N}$:Si layer, which has the smallest bandgap across the optical path.

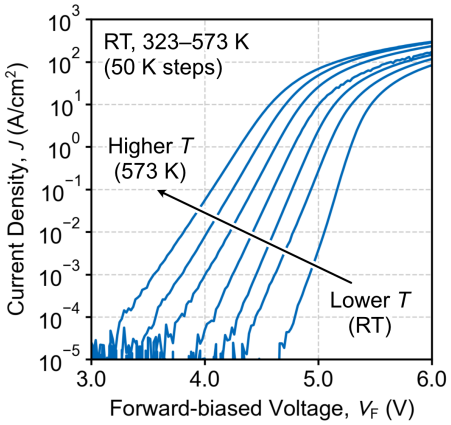

Fig. 10. Temperature-dependent forward-biased *J*–*V* characteristic of the fabricated diode. The temperatures were set to RT and 323–573 K with 50 K steps.

The minimum n value was 1.8 at RT and remained around 2.0 at any temperature, indicating that the forward-biased *J*–*V* characteristics can be described by the recombination current model. The results show that the fabricated diode is the "true" PND and not one that coincidentally exhibits a reasonable ideality factor.

The reverse-biased *J*–*V* characteristic of the fabricated diode is shown in Fig. 12(a). The device showed a destructive breakdown at −283 V, and uniform avalanche breakdown did not occur in this device. The corresponding parallel-plane breakdown electric field was calculated with respect to the electric field distribution both in p-type and n-type layers. In the double-side depleted p-n diodes, the breakdown electric field (E_{B}) can be expressed as

$$E_{\mathrm{B}} = \frac{V_{\mathrm{B}}}{t_p + t_n} + \frac{q}{2\epsilon_{\mathrm{s}}} \frac{N^+_{\mathrm{DPD}} t_n^2 + N^-_{\mathrm{DPD}} t_p^2}{t_p + t_n}, \tag{2}$$

where V_{B} is the breakdown voltage, t_p and t_n are the thicknesses of p-type and n-type layers, respectively, and ϵ_{s} is the permittivity of the semiconductor. Applying $t_p = 70$ nm, $t_n = 380$ nm, $N^-_{\mathrm{DPD}} = 1.8 \times 10^{18}$ cm^{-3}, and $N^+_{\mathrm{DPD}} = 2.6 \times 10^{17}$ cm^{-3} with respect to the SIMS result, we calculated E_{B} as 7.3 MV cm^{-1}. It is worth emphasizing that the thicknesses and doping concentrations of p$^+$-DPD AlGaN and n-DPD AlGaN layers determined by SIMS measurement (i.e., the values used for the calculation of E_{B}) are consistent with those determined by TEM and *C*–*V* measurements. The E_{B} value is approximately twice as high as that reported for the GaN limit at the same doping concentration ($N = 2.6 \times 10^{17}$ cm^{-3}), whereas the fabricated p$^+$-n diode still does not fully demonstrate the potential of high-Al-content AlGaN owing to the absence of an appropriate edge termination structure [28].

One performance limiting factor is the significant leakage current; hence, its origin was investigated by photo emission microscopy. Fig. 12(b) shows the photo emission microscopy image of a "typical" fabricated diode near breakdown voltage [not the same diode as that shown in Fig. 12(a)]. The leakage current was found to flow non-uniformly, being concentrated at several specific points. In the case of GaN p-n diodes, the origin of the spotty current leakage observed by the same method is reported to be (threading) dislocations, which primarily originated from substrates [29]. However, this theory is hard to apply to this study since the fabricated diode should not contain any dislocations, as statistically estimated from the TDD of the substrate (10^3–10^4 cm^{-2}). This implies that dislocations are likely newly generated during device fabrication processes. Therefore, the area near the mesa edge of the diode was observed by TEM. Fig. 13 shows the plan-

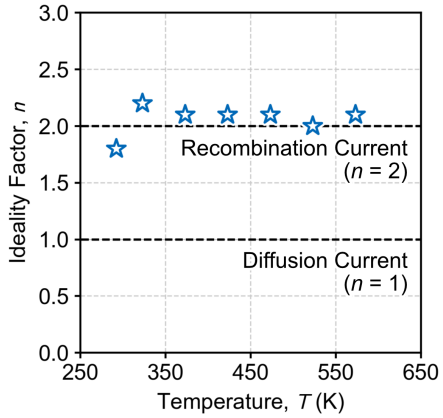

Fig. 11. Temperature-dependent ideality factor extracted from the forward-biased *J*–*V* characteristics.

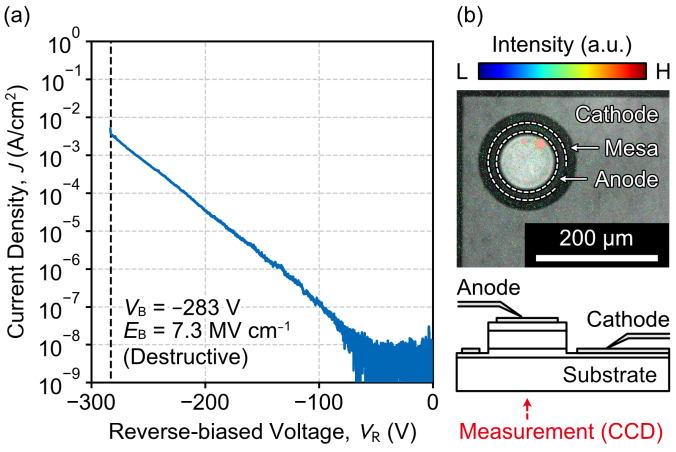

Fig. 12. (a) Reverse-biased *J*–*V* characteristic of the best-performance fabricated diode at RT. The breakdown voltage varied from $-\mathbf{206}$ to $-\mathbf{283}$ V across different devices on this chip, with a total of 12 devices being tested. (b) Photo emission microscopy image of a fabricated "typical" diode under reverse-biased voltage ($\boldsymbol{V_R}$) of $-\mathbf{257}$ V (near breakdown voltage). The inset shows the measurement setup.

view TEM image of a fabricated diode. Numerous dislocation lines, which appear black in contrast, were observed along the mesa edge. Kushimoto *et al.* also observed similar dislocation lines in the UV-C laser diode structure with DPD on AlN substrates [30]. They conducted a comprehensive investigation into the causes of dislocation formation during device fabrication processes and also offered solutions to address this issue. Due to lattice mismatch, AlGaN layers pseudomorphically grown on AlN substrates experience significant compressive stress. Although the stress distribution within the plain wafer is uniform, shear stress is generated if mesa structures are formed on such wafers and concentrated particularly at the mesa corners. Since the yield stress decreases with increasing temperature, dislocations are newly generated owing to the shear stress during high-temperature processes such as activation and sintering annealing. Consequently, the dislocations observed in TEM analysis, which align spatially with the leak spots identified in photoemission spectroscopy analysis, are plausible candidates for the reverse leakage current. This

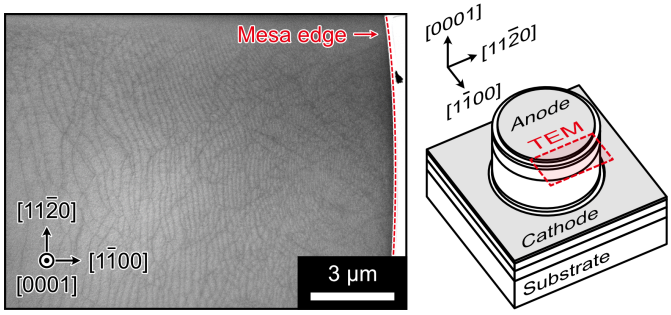

Fig. 13. Plan-view TEM image of a fabricated diode. The dark lines indicate dislocations. The inset shows the schematic of a diode, including the area analyzed by TEM.

suggests that negatively beveled mesa structures mitigating local shear stress concentration, such as UV-C laser diodes and/or low-temperature device fabrication processes, have the potential to suppress the dislocation generation and improve reverse-biased *J*–*V* characteristics.

IV. Conclusion

In this study, we investigated AlN-based vertical p-n diodes fabricated utilizing dopant-free DPD for both p- and n-type layers to resolve impurity-doping-related problems in AlN-based materials. The net charge concentration extracted from *C*–*V* measurements agreed well with that expected from the compositional gradient measured by SIMS. The forward-biased *J*–*V* characteristics exhibited a specific ON-resistance of 3 mΩ cm^2 and a turn-on voltage of 6.5 V, which were the smallest among the reported AlN-based PNDs, as well as EL emissions with a photon energy of around 5.1 eV (240 nm). Detailed analyses of the resistance components in the fabricated diode indicated that the current limitation on the ON-resistance is predominantly due to the spreading resistance in the n$^+$-$Al_{0.7}Ga_{0.3}N$:Si layer. The fabricated devices also showed a record-low ideality factor of 1.8 at room temperature, which remained around 2.0 across elevated temperatures. The breakdown electric field recorded was 7.3 MV cm^{-1}, which is twice as high as the reported critical electric field of GaN, despite the absence of edge termination structures. The origin of the reverse leakage in these devices was discussed on the basis of TEM analysis, and the device mesa structure and/or fabrication process (rather than epitaxial growth) optimizations are found to be one pathway to improving the device performance. These results prove DPD's effectiveness for AlN-based materials to overcome its technical limits and the great potential of "semiconducting" AlN in power device applications.

Acknowledgment

The authors express their sincere appreciation to Professor Leo J. Schowalter of Nagoya University, as well as Dr. Ziyi Zhang, Dr. Takaharu Nagatomi, Mr. Sho Sugiyama, and Dr. Naohiro Kuze of Asahi Kasei Corporation for their invaluable discussions, analyses, and considerable supports. Additionally, the authors wish to thank Mr. Koji Aoto, Dr. Katsunori

Nishii, and the working members of the Center for Integrated Research of Future Electronics (CIRFE) Transformative Electronics Facilities (C-TEFs) of Nagoya University for their great contributions to device fabrications. Takeru Kumabe acknowledges Ms. Shivali Agrawal, Professor Huili Xing, and Professor Debdeep Jena of Cornell University for their invaluable discussions.

REFERENCES

[1] R. J. Kaplar, A. A. Allerman, A. M. Armstrong, M. H. Crawford, J. R. Dickerson, A. J. Fischer, A. G. Baca, and E. A. Douglas, "Review—Ultra-Wide-Bandgap AlGaN Power Electronic Devices," *ECS J. Solid State Sci. Technol*, vol. 6, no. 2, Q3061–Q3066, Dec. 2016, doi:10.1149/2.0111702jss.

[2] J. Y. Tsao, S. Chowdhury, M. A. Hollis, D. Jena, N. M. Johnson, K. A. Jones, R. J. Kaplar, S. Rajan, C. G. Van de Walle, E. Bellotti, C. L. Chua, R. Collazo, M. E. Coltrin, J. A. Cooper, K. R. Evans, S. Graham, T. A. Grotjohn, E. R. Heller, M. Higashiwaki, M. S. Islam, P. W. Juodawlkis, M. A. Khan, A. D. Koehler, J. H. Leach, U. K. Mishra, R. J. Nemanich, R. C. N. Pilawa-Podgurski, J. B. Shealy, Z. Sitar, M. J. Tadjer, A. F. Witulski, M. Wraback, and J. A. Simmons, "Ultrawide-Bandgap Semiconductors: Research Opportunities and Challenges," *Adv. Electron. Mater.*, vol. 4, issue 1, 1600501, Jan. 2018, doi:10.1002/aelm.201600501.

[3] R. T. Bondokov, S. G. Mueller, K. E. Morgan, G. A. Slack, S. Schujman, M. C. Wood, J. A. Smart, and L. J. Schowalter, 'Large-area AlN substrates for electronic applications: An industrial perspective," *J. Cryst. Growth*, vol. 310, issue 17, pp. 4020–4026, Jun. 2008, doi:10.1016/j.jcrysgro.2008.06.032.

[4] P. Lu, R. Collazo, R. F. Dalmau, G. Durkaya, N. Dietz, B. Raghothamachar, M. Dudley, and Z. Sitar, 'Seeded growth of AlN bulk crystals in *m*- and *c*-orientation," *J. Cryst. Growth*, vol. 312, issue 1, pp. 58–63, Dec. 2009, doi:10.1016/j.jcrysgro.2009.10.008.

[5] H. Helava, T. Chemekova, O. Avdeev, E. Mokhov, S. Nagalyuk, Y. Makarov, and M. Ramm, 'AlN substrates and epitaxy results," *Phys. Status Solidi C*, vol. 7, issue 7–8, pp. 2115–2117, Jul. 2010, doi:10.1002/pssc.200983619.

[6] M. Bickermann, B. M. Epelbaum, O. Filip, P. Heimann, S. Nagata, and A. Winnacker, "UV transparent single-crystalline bulk AlN substrates," *Phys. Status Solidi C*, vol. 7, issue 1, pp. 21–24, Jan. 2010, doi:10.1002/pssc.200982601.

[7] Y. Irokawa, E. A. García Víllora, and K. Shimamura, "Shottky barrier diodes on AlN free-standing substrates," *Jpn. J. Appl. Phys.*, vol. 51, no. 4R, 040206, Mar. 2012, doi:10.1143/JJAP.51.040206.

[8] R. Dalmau, H. Spalding Craft, R. Schlesser, S. Mita, J. Smart, C. Hitchcock, G. Pandey, T. P. Chow, and B. Moody, "Progress and challenges of AlGaN Schottky diodes grown on AlN substrates," *ECS Trans.*, vol. 80, no. 7, pp. 217–226, 2017, doi:10.1149/08007.0217ecst.

[9] T. Maeda, R. Page, K. Nomoto, M. Toita, H. G. Xing, and D. Jena, "AlN quasi-vertical Schottky barrier diode on AlN bulk substrate using $Al_{0.9}Ga_{0.1}N$ current spreading layer," *Appl. Phys. Express*, vol. 15, no. 6, 061007, May 2022, doi:10.35848/1882-0786/ac702e.

[10] Y. Taniyasu, M. Kasu, and N. Kobayashi, "Intentional control of n-type conduction for Si-doped AlN and $Al_xGa_{1-x}N$ ($0.42 \leq x < 1$)," *Appl. Phys. Lett.*, vol. 81, no. 7, pp. 1255–1257, Aug. 2002, doi:10.1063/1.1499738.

[11] Y. Taniyasu, M. Kasu, and T. Makimoto, "Electrical conduction properties of n-type Si-doped AlN with high electron mobility (> 100 cm^2 V^{-1} s^{-1})," *Appl. Phys. Lett.*, vol. 85, no. 20, pp. 4672–4674, Nov. 2004, doi:10.1063/1.1824181.

[12] Y. Taniyasu, M. Kasu, and T. Makimoto, "An aluminium nitride light-emitting diode with a wavelength of 210 nanometres," *Nature*, vol. 441, no. 7091, pp. 325–328, May 2006, doi:10.1038/nature04760.

[13] B. Sarkar, S. Washiyama, M. Hayden Breckenridge, A. Klump, J. N. Baker, P. Reddy, J. Tweedie, S. Mita, R. Kirste, D. L. Irving, R. Collazo, and Z. Sitar, "N- and P- type Doping in Al-rich AlGaN and AlN," *ECS Trans.*, vol. 86, no. 12, pp. 25–30, 2018, doi:10.1149/MA2018-02/38/1283.

[14] K. Kataoka, T. Narita, Y. Yagi, K. Nagata, and Y. Saito, "Comprehensive study of electron conduction and its compensation for degenerate Si-doped AlN-rich AlGaN," *Phys. Status Solidi RRL*, 2300055, Jun. 2023, doi:10.1002/pssr.202300055.

[15] D. Jena, S. Heikman, D. Green, D. Buttari, R. Coffie, H. Xing, S. Keller, S. DenBaars, J. S. Speck, and U. K. Mishra, "Realization of wide electron slabs by polarization bulk doping in graded Ⅲ–Ⅴ nitride semiconductor alloys," *Appl. Phys. Lett.*, vol. 81, no. 23, pp. 4395–4397, Dec. 2002, doi:10.1063/1.1526161.

[16] T. Kumabe, S. Kawasaki, H. Watanabe, S. Nitta, Y. Honda, and H. Amano, "Space charge profiles and carrier transport properties in dopant-free GaN-based p-n junction formed by distributed polarization doping," *Phys. Status Solidi RRL*, vol. 16, issue 7, 2200127, May 2022, doi:10.1002/pssr.202200127.

[17] T. Kumabe, S. Kawasaki, H. Watanabe, Y. Honda, and H. Amano, "Hole mobility limiting factors in dopant-free p-type distributed polarization-doped AlGaN," *Appl. Phys. Lett.*, vol. 122, no. 25, 252107, Jun. 2023, doi:10.1063/5.0155363.

[18] T. Kumabe, S. Kawasaki, H. Watanabe, Y. Honda, and H. Amano, "Electron lifetime and diffusion coefficient in dopant-free p-type distributed polarization doped AlGaN," *Appl. Phys. Lett.*, vol. 123, no. 25, 252101, Dec. 2023, doi:10.1063/5.0180062.

[19] Z. Zhang, M. Kushimoto, A. Yoshikawa, K. Aoto, C. Sasaoka, L. J. Schowalter, and H. Amano, "Key temperature-dependent characteristics of AlGaN-based UV-C laser diode and demonstration of room-temperature continuous-wave lasing," *Appl. Phys. Lett.*, vol. 121, no. 22, 222103, Nov. 2022, doi:10.1063/5.0124480.

[20] A. Nishikawa, K. Kumakura, T. Akasaka, and T. Makimoto, "High critical electric field of $Al_xGa_{1-x}N$ p-i-n vertical conducting diodes on n-SiC substrates," *Appl. Phys. Lett.*, vol. 88, no. 17, 173508, Apr. 2006, doi:10.1063/1.2198092.

[21] A. Nishikawa, T. Akasaka, and T. Makimoto, "High critical electric field exceeding 8 MV/cm measured using an AlGaN p–i–n vertical conducting diode on n-SiC substrate," *Jpn. J. Appl. Phys.*, vol. 46, no. 4B, pp. 2316–2319, Apr. 2007, doi:10.1143/JJAP.46.2316.

[22] A. Nishikawa, K. Kumakura, M. Kasu, and T. Makimoto, "High-temperature characteristics of $Al_xGa_{1-x}N$-based vertical conducting diodes," *Jpn. J. Appl. Phys.*, vol. 47, no. 4, pp. 2838–2840, Apr. 2008, doi:10.1143/JJAP.46.2316.

[23] A. A. Allerman, A. M. Armstrong, A. J. Fischer, J. R. Dickerson, M. H. Crawford, M. P. King, M. W. Moseley, J. J. Wierer, R.J. Kaplar, "$Al_{0.3}Ga_{0.7}N$ PN diode with breakdown voltage ¿1600 V," *Electron. Lett.*, vol. 52, issue 15, pp. 1319–1321, Jul. 2016, doi:10.1049/el.2016.1280.

[24] H. Ahmad, Z. Engel, C. M. Matthews, S. Lee, and W. A. Doolittle, "Realization of homojunction PN AlN diodes," *J. Appl. Phys.*, vol. 131, no. 17, 175701, May 2022, doi:10.1063/5.0086314.

[25] R. T. Bondokov, S. P. Branagan, N. Ishigami, J. Grandusky, T. Nagatomi, K. Tatsuta, T. Miebach, and J. Chen, *ECS Trans.*, vol. 104, no. 7, pp. 37–48, 2021, doi:10.1149/10407.0037ecst.

[26] T. Sakai, M. Kushimoto, Z. Zhang, N. Sugiyama, L. J. Schowalter, Y. Honda, C. Sasaoka, and H. Amano, "On-wafer fabrication of etched-mirror UV-C laser diodes with the ALD-deposited DBR," *Appl. Phys. Lett.*, vol. 116, no. 12, 122101, Mar. 2020, doi:10.1063/1.5145017.

[27] T. Kumabe, Y. Ando, H. Watanabe, M. Deki, A. Tanaka, S. Nitta, Y. Honda, and H. Amano, "Etching-induced damage in heavily Mg-doped p-type GaN and its suppression by low-bias-power inductively coupled plasma-reactive ion etching," *Jpn. J. Appl. Phys.*, vol. 60, no. SB, SBBD03, Jan. 2021, doi:10.35848/1347-4065/abd538.

[28] T. Maeda, T. Narita, S. Yamada, T. Kachi, T. Kimoto, M. Horita, and J. Suda, "Impact ionization coefficients and critical electric field in GaN," *J. Appl. Phys.*, vol. 129, no. 18, 185702, May 2021, doi:10.1063/5.0050793.

[29] S. Usami, Y. Ando, A. Tanaka, K. Nagamatsu, M. Deki, M. Kushimoto, S. Nitta, Y. Honda, H. Amano, Y. Sugawara, Y.-Z. Yao, Y. Ishikawa, "Correlation between dislocations and leakage current of p-n diodes on a free-standing GaN substrate," *Appl. Phys. Lett.*, vol. 112, no. 18, 182106, Apr. 2018, doi:10.1063/1.5024704.

[30] M. Kushimoto, Z. Zhang, A. Yoshikawa, K. Aoto, Y. Honda, C. Sasaoka, L. J. Schowalter, and H. Amano, "Local stress control to suppress dislocation generation for pseudomorphically grown AlGaN UV-C laser diodes," *Appl. Phys. Lett.*, vol. 121, no. 22, 222101, Nov. 2022, doi:10.1063/5.0124512.